RSC Advances

PAPER

View Article Online
View Journal | View Issue

Cite this: *RSC Adv.*, 2017, **7**, 15053

Low-cost dual cocatalysts $BiVO_4$ for highly efficient visible photocatalytic oxidation

Feng Lin,[a] Zhiyu Shao,[a] Ping Li,[bc] Zhenpan Chen,[bc] Xinyi Liu,[bc] Mingrun Li,[bc] Bao Zhang,[bc] Jindou Huang,[a] Guangqi Zhu*[bc] and Bin Dong*[a]

Received 30th November 2016
Accepted 5th February 2017

DOI: 10.1039/c6ra27559a

rsc.li/rsc-advances

The cocatalysts of noble metals are reported to play a significant role in improving the photocatalytic activity in water splitting and pollutant degradation reactions. The high price of noble metals limits their further application in industry. Herein, for the first time, we report that thiophene, rhodamine B (RhB) and methyl orange (MO) can be efficiently oxidized on $BiVO_4$ co-loaded with Ni and CuO cocatalysts (denoted as Ni–CuO/$BiVO_4$) under visible light irradiation with molecular oxygen as the oxidant. Moreover, 0.05 wt% Ni–0.5 wt% CuO/$BiVO_4$ possesses high photocatalytic activity (over 94% conversion of thiophene), which is close to Pt–RuO_2/$BiVO_4$ (99% conversion of thiophene). XPS and ESR measurements showed that the activation of molecular oxygen and oxidation of pollutant molecules simultaneously take place on $BiVO_4$ co-loaded with Ni/Cu and CuO/Cu_2O cocatalysts. The considerable enhancement of photocatalytic activity can be attributed to the simultaneous presence of the reduction cocatalyst Ni/Cu and oxidation cocatalyst CuO/Cu_2O, which are beneficial for the efficient separation and transfer of the photo-generated electrons and holes. Such visible-light-responsive semiconductor loaded with earth-abundant dual cocatalysts has great potential in both solar energy conversion and further industrial applications.

1. Introduction

Solar driven catalysis on semiconductors is widely considered as a promising route to mitigate environmental issues caused by the combustion of fossil fuels and to meet increasing worldwide demands for energy.[1,2] SO_x produced from the automobile exhaust gas *via* the burning of sulfur-containing components present in fuels results in serious air pollution. Among the sulfur-containing components, thiophene, with the aromaticity and the low electron density of the sulfur atom, is most difficult to oxidize with conventional oxidative desulfurization processes.[3] Some effective photocatalysts have been reported for the removal of sulfur-containing compounds in gasoline *via* photocatalytic oxidation.[4–7] Polluted waste water from industry is a global environmental issue. The azo dyes rhodamine B (RhB) and methyl orange (MO) are widely used for coloring textiles. Consequently, several materials that enable the cleanup of polluted water *via* a far less aggressive approach have been developed.[8,9]

The major restriction factors affecting the efficiency of photocatalysis include (i) light absorption, (ii) charge separation and transport and (iii) surface chemical reaction. In recent years, some visible-light-responsive bulk semiconductors[10–15] were investigated in photocatalytic water splitting and pollutants degradation reaction, such as WO_3, $BiVO_4$, Bi_2WO_6, $CaBi_2O_4$, $Bi_2Ti_2O_7$, and Ag_3PO_4. These semiconductors can expand the light absorption of photocatalysts to the visible light region, which is far beyond the light absorption of TiO_2. In order to improve the efficiency of photocatalysis, a promising strategy is to load cocatalysts or secondary semiconductors that can act as either electron or hole acceptors for improved charge separation.[16,17] Since the early report of CdS loaded with dual cocatalysts Pt and PdS by Can Li, which can achieve an extremely high QE (93%) in photocatalytic H_2 production,[18] there have been few investigations on the effect of dual cocatalysts in photocatalytic reactions. In our previous study, thiophene could be oxidized to SO_3 on $BiVO_4$ co-loaded with Pt and RuO_2 cocatalysts under visible light irradiation with molecular oxygen as the oxidant.[5] Domen *et al.* synthesized WO_3 co-loaded with Pt and RuO_2 cocatalysts and investigated the performance in the photocatalytic IO_3^- reduction and water oxidation.[19] The reports show that the synergistic effect between suitable cocatalysts on the photocatalytic activity is very important to the photocatalytic reaction. However, the high price of noble metals limits further application in industry. The exploration of earth-abundant elements cocatalysts in photocatalytic reactions is highly desired.

Recently, some abundant and low-cost materials have been reported to replace noble metal catalysts for photocatalysis. Domen *et al.* prepared $CuCrO_x$/GaN:ZnO composite

[a]*Key Laboratory of New Energy and Rare Earth Resource Utilization, State Ethnic Affairs Commission, School of Physics and Materials Engineering, Dalian Nationalities University, Dalian, 116600, China. E-mail: dong@dlnu.edu.cn; linfeng@dlnu.edu.cn; Fax: +86-411-87658872; Tel: +86-411-87556959*

[b]*State Key Laboratory of Catalysis, Dalian Institute of Chemical Physics, Chinese Academy of Sciences, 457 Zhongshan Road, Dalian 116023, China*

[c]*Dalian National Laboratory for Clean Energy, Dalian 116023, China*

photocatalyst[20] with its photocatalytic activity being 25–30% the activity of $Rh_{2-y}Cr_yO_3$/GaN:ZnO. Using earth-abundant element Cu, a cheap and efficient photocatalyst can be obtained. Ghim Wei Ho *et al.* loaded a core–shell structure Cu–CuO cocatalyst on TiO_2 (ref. 21) to achieve a high photocatalytic activity of H_2 production, which was attributed to the promoted charge separation and transport. Moreover, Co doped $BiVO_4$ (ref. 22) and $LaTiO_2N$[23] are reported to perform well in photocatalytic degradation and water oxidation reactions. Other cocatalysts, such as Ni, NiO, $Ni(OH)_2$ and NiS,[24–27] were also studied for photocatalysis, but the activities and stability were much lower than those of the two systems mentioned above.[28,29] These studies show that although the enhanced activity on noble-metal-free cocatalyst is lower than that on the noble metals, the earth-abundant elements have great potential in both theory and industry. The suitable noble-metal-free dual cocatalysts may enhance the photocatalytic activity significantly. However, little research has been reported on the effect of the dual cocatalysts on the photocatalytic activity of a $BiVO_4$-based photocatalyst for photocatalytic waste oxidation.[5] Moreover, the synergistic effect of low-cost dual cocatalysts is far less investigated in photocatalysis for environmental protection.

Herein, we report the photocatalytic oxidation of thiophene, RhB and MO by a visible-light responsive photocatalyst Ni–CuO/$BiVO_4$. We found that $BiVO_4$ co-loaded with Ni and CuO showed a strong synergistic effect between the two cocatalysts on the photocatalytic activity of thiophene oxidation and pollutant degradation. A high photocatalytic activity close to Pt–RuO_2/$BiVO_4$ could be achieved under visible light irradiation ($\lambda \geq 420$ nm) using molecular oxygen as the oxidant.

2. Experimental

2.1 Catalyst preparation

All chemicals in these experiments were of analytical reagent grade and used without further treatment. $BiVO_4$ samples were synthesized according to our previous study,[5] while $BiVO_4$ (i) corresponds to the pH value of the resulting solution adjusted to *i* with ammonia solution ($i = 2.0$, 4.0, 9.0).

The loading of copper oxide on $BiVO_4$ (2) was performed by the impregnation method. $Cu(NO_3)_2$ was used as the precursor. $BiVO_4$ powder was impregnated in an aqueous solution containing a given amount of $Cu(NO_3)_2$. The solution was then evaporated over a water bath at 80 °C, followed by calcination in air at 350 °C for 4 h. Metal nickel was co-loaded onto CuO/$BiVO_4$ by the photo deposition method. The photocatalyst, $BiVO_4$ (2) co-loaded with the metal Ni and metal oxide CuO was denoted as Ni–CuO/$BiVO_4$.

2.2 Catalyst characterization

The catalysts were characterized by X-ray powder diffraction (XRD) on a Rigaku D/Max-2500/PC powder diffractometer. Each sample was scanned using Cu-K_α radiation with an operating voltage of 40 kV and an operating current of 200 mA. A scan rate of 5° min^{-1} was applied to record the patterns in the range of 10°–80° at a step of 0.02°.

UV-Visible diffuse reflectance spectra (UV-Vis DRS) were recorded on a UV-Vis spectrophotometer (PerkinElmer Lambda 750) equipped with an integrating sphere. The morphologies and particle sizes were examined by scanning electron microscopy (SEM) equipped with a Quanta 200 FEG scanning electron microscope with a 0.5–30 kV accelerating voltage. High-resolution transmission electron microscopy (HRTEM) images, scanning transmission electron microscopy (STEM) images and energy dispersive spectroscopy (EDS) were obtained on a Tecnai G2 F30 S-Twin (FEI Company) instrument.

X-ray photoelectron spectroscopy (XPS) was acquired on a Thermo ESCALAB 250Xi with an Al Kα X-ray ($h\nu = 1486.6$ eV). Base pressure in the analysis chamber was maintained at 10^{-8} Pa. Energy resolution of the spectrometer was set at 0.8 eV at a pass energy of 20 eV. Full width at half maximum (FWHM) was calibrated with respect to Ag $3d_{5/2}$ FWHM at 0.65 eV. The error in all the BE values reported was 0.22 eV.

ESR signals of radicals trapped by DMPO were recorded at ambient temperature on a Brucker ESR A200 spectrometer. After bubbling O_2 for 10 min, the samples were introduced into the homemade quartz cup inside the microwave cavity and illuminated with a 300 W Xe lamp (CERAMAX LX-300). The settings for the ESR spectrometer were as follows: center field, 3486.70 G; sweep width, 100 G; microwave frequency, 9.82 GHz; modulation frequency, 200 kHz; power, and 10.00 mW. Magnetic parameters of the radicals detected were obtained from direct measurements of magnetic field and microwave frequency.

2.3 Photocatalytic reaction

The photocatalytic reactions of thiophene were carried out in a Pyrex reaction cell with O_2 or air bubbled in a constant flow. Photocatalyst (1 g L^{-1}) was dispersed in an acetonitrile solution containing given amounts of thiophene ($[\text{sulfur content}]_{\text{initial}} = 600$ ppm). The suspension was irradiated by a 300 W Xe lamp (CERAMAX LX-300) equipped with an optical filter ($\lambda \geq 420$ nm) to cut off the light in the ultraviolet region. The temperature of the reaction solution was maintained at 10 °C ± 2 °C by a flow of cooling water. The products were analyzed by GC-FPD (Agilent 7890, pona column).

The photocatalytic degradation reactions of dyes rhodamine B (RhB) and methyl orange (MO) were carried out in a Pyrex reaction cell. Photocatalyst (1 g L^{-1}) was dispersed in an aqueous solution containing given amounts of the pollutants ($C_0 = 5$ ppm). The temperature of the reaction solution was maintained at 10 °C ± 2 °C by a flow of cooling water. The concentration of RhB and MO was monitored by colorimetry with a JASCO V-550 UV-vis spectrometer. The λ_{max} for RB and MO are 553 and 467 nm, respectively. Calibration based on the Beer–Lambert law was used to quantify the dye concentration.

3. Results and discussion

3.1 Characterization of catalysts

Fig. 1 shows the morphology of $BiVO_4$ samples synthesized under different experimental conditions and loaded with cocatalysts. SEM images present several morphologies for

$BiVO_4$ that are also reported in other studies.[30,31] As shown in Fig. 1, large compact particles (about 2 μm in size) of decagonal shape are observed for $BiVO_4$ (2). The particles show a smooth surface and well-defined edges. The $BiVO_4$ (4) sample exhibited a polyhedral shape with the size of about 3 μm.

The $BiVO_4$ (9) sample showed a trunk shape. We investigated the photocatalytic thiophene oxidation on these $BiVO_4$ samples, and the conversion of thiophene in 3 h on $BiVO_4$ (2), $BiVO_4$ (4) and $BiVO_4$ (9) was *ca.* 40%, 12% and 16%, respectively. As $BiVO_4$ (2) was much more photoactive than $BiVO_4$ (4) and $BiVO_4$ (9), $BiVO_4$ (2) was synthesized to load with cocatalysts for the following experiments. In the following discussion, $BiVO_4$ represents $BiVO_4$ (2). After loading cocatalysts CuO and Ni, the nanoparticles were highly dispersed on the smooth surface of $BiVO_4$ for CuO/$BiVO_4$ and Ni–CuO/$BiVO_4$ (as shown in Fig. 1).

Fig. 2 shows the HRTEM (STEM) images and EDS analysis for the microstructure of the catalysts CuO/$BiVO_4$ and Ni–CuO/$BiVO_4$. The images (Fig. 2a and b) show that CuO loaded on $BiVO_4$ was mainly in the form of semispherical particles. The typical particle size of CuO is estimated to be about 5–10 nm. For Ni–CuO/$BiVO_4$ catalyst (Fig. 2d and e), Ni nanoparticles were dispersed on the surface of $BiVO_4$ in the form of flat spheres besides CuO. The typical particle size of Ni is estimated to be about 2–6 nm. In addition, the EDS analysis revealed the presence of Cu on both CuO/$BiVO_4$ and Ni–CuO/$BiVO_4$ (Fig. 2c and f).

$BiVO_4$ prepared by hydrothermal treatment is a monoclinic scheelite according to the standard card no. 14-0688 (Fig. 3a). After loading cocatalysts CuO and Ni, there was no evident diffraction peak of elements Cu or Ni. The XRD pattern of the Ni–CuO/$BiVO_4$ sample demonstrated the monoclinic phase. Fig. 3b shows the UV-vis diffuse reflectance spectra of $BiVO_4$ and Ni–CuO/$BiVO_4$. $BiVO_4$ showed strong absorption in the UV light region and the visible light region until 535 nm. The band gap of $BiVO_4$ is estimated to be 2.3 eV from the absorption edge of the UV-vis DRS. After loading cocatalysts onto $BiVO_4$, no evident shift of the absorption edge was observed. Consequently, Ni–CuO/$BiVO_4$ can absorb light ($\lambda \geq 400$ nm) beyond the absorption edges of gasoline and light diesel.[5]

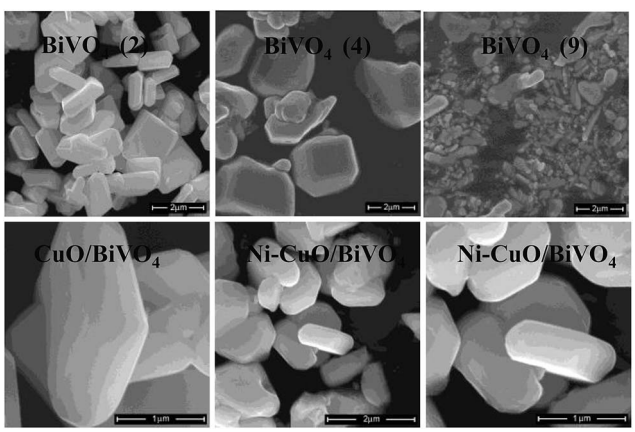

Fig. 1 SEM images of $BiVO_4$ (2), $BiVO_4$ (4), $BiVO_4$ (9), CuO/$BiVO_4$ and Ni–CuO/$BiVO_4$.

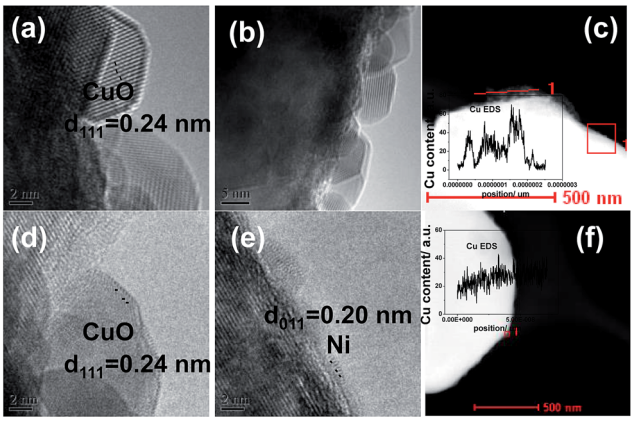

Fig. 2 HRTEM images of (a) and (b) CuO/$BiVO_4$, (d) and (e) Ni–CuO/$BiVO_4$. STEM images and EDS analysis of (c) CuO/$BiVO_4$, (f) Ni–CuO/$BiVO_4$.

3.2 The effect of cocatalysts on photocatalytic oxidation reaction

3.2.1 The photocatalytic oxidation of rhodamine B (RhB) and methyl orange (MO). The effect of the photocatalytic oxidation activity of RhB on the loadings of CuO on $BiVO_4$ is shown in Fig. 4a. The residual RhB concentration (C/C_0) for 2.5 h reaction is *ca.* 22% on bare $BiVO_4$. For CuO/$BiVO_4$ catalyst, as the loading of Cu increased from 0 to 0.5 wt%, the photocatalytic oxidation activity of RhB was significantly enhanced. RhB could be completely degraded in 1.5 h under visible light irradiation on 0.5 wt% CuO/$BiVO_4$. On the other hand, the photocatalytic oxidation activity of CuO/$BiVO_4$ was almost the same when the loadings of Cu varied from 0.5 to 0.9 wt%. Namely, the extra amount of Cu loaded onto $BiVO_4$ was not necessary. The loading of Cu was set to 0.5 wt% to optimize the photocatalytic oxidation activity for RhB by varying the amount of the co-loaded Ni. As shown in Fig. 4b, the photocatalytic oxidation activity could be greatly improved when the loading of Ni was varied from 0 to 0.05 wt%. As the loading of co-loaded Ni

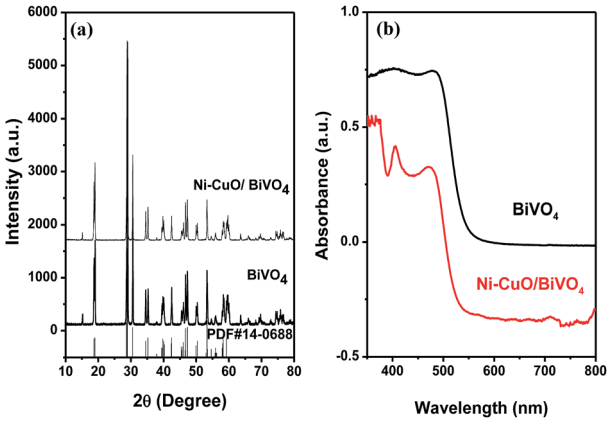

Fig. 3 (a) XRD patterns of Ni–CuO/$BiVO_4$, $BiVO_4$ and the standard card of $BiVO_4$ (no. 14-0688). (b) UV-Vis DRS of $BiVO_4$ and of Ni–CuO/$BiVO_4$ photocatalyst.

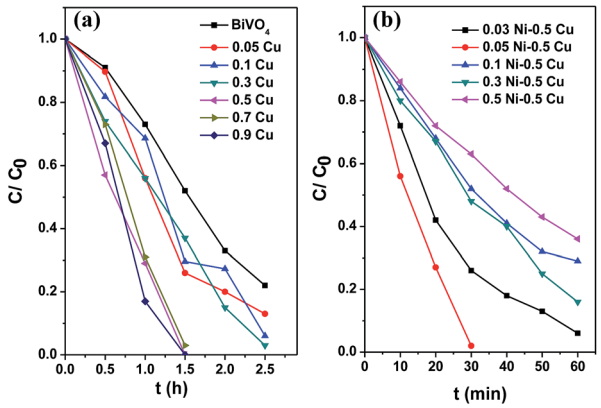

Fig. 4 Photocatalytic oxidation of RhB on $BiVO_4$ loaded with cocatalysts (a) CuO and (b) Ni–CuO. Herein 0.05 Cu represents 0.05 wt% CuO/$BiVO_4$, 0.03Ni–0.5 Cu represents 0.03 wt% Ni–0.5 wt% CuO/$BiVO_4$, and so on. Reaction conditions: the concentration of photocatalyst: 1 g L^{-1}; the initial concentration of RhB, C_0 = 5 ppm; light source: 300 W Xe lamp (CERAMAX LX-300, $\lambda \geq 420$ nm); temperature: 10 ± 2 °C.

increased to 0.05 wt%, RhB could be completely degraded in 0.5 h under visible light irradiation. The complete degradation of RhB on 0.1–0.5 wt% Ni–0.5 wt% CuO/$BiVO_4$ required over 70 min. Consequently, the 0.05 wt% Ni–0.5 wt% CuO/$BiVO_4$ photocatalyst exhibited the highest photocatalytic activity for RhB degradation under visible light irradiation. In addition, Fig. 5 shows the photocatalytic behaviours for degradation of MO under the same conditions. The photocatalytic activity could be greatly enhanced on 0.05 wt% Ni–0.5 wt% CuO/$BiVO_4$. MO could be completely degraded within 20 min under visible light irradiation. These results imply that the photocatalytic activity for degrading RhB and MO on $BiVO_4$ can be significantly improved by co-loading noble-metal-free dual cocatalysts Ni and CuO. The synergistic effect between suitable cocatalysts on the photocatalytic activity is important to the photocatalytic oxidation degradation of dyes.

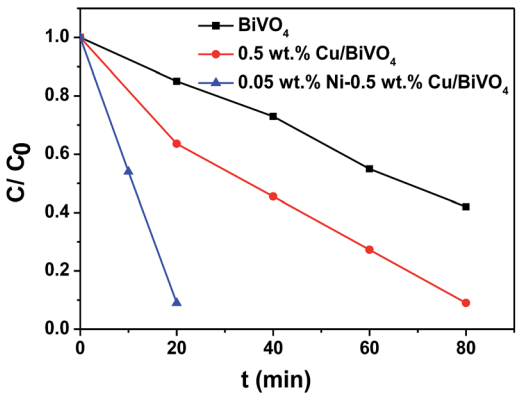

Fig. 5 Photocatalytic oxidation of MO on $BiVO_4$ loaded with cocatalysts Ni and CuO. Reaction conditions: the concentration of photocatalyst: 1 g L^{-1}; the initial concentration of MO, C_0 = 5 ppm; light source: 300 W Xe lamp (CERAMAX LX-300, $\lambda \geq 420$ nm); temperature: 10 ± 2 °C.

3.2.2 The photocatalytic oxidation of thiophene. Fig. 6 shows the conversion for photocatalytic oxidation of thiophene on $BiVO_4$, Ni/$BiVO_4$, CuO/$BiVO_4$, Ni–CuO/$BiVO_4$, CoO_x/$BiVO_4$, Ni–CoO_x/$BiVO_4$, NiO_x/$BiVO_4$ and Co–NiO_x/$BiVO_4$ photocatalysts. Generally, the ultra-low loading of cocatalyst should be adopted for all the cocatalysts to study the intrinsic effect of the cocatalyst. However, for noble-metal-free cocatalyst, the photocatalytic activity cannot be improved considerably with only 0.01 wt% cocatalyst loading. Thus, we conclude the photocatalytic oxidation activity of thiophene on $BiVO_4$ loaded with an optimized amount of cocatalysts. $BiVO_4$ without the cocatalysts exhibited low conversion for photocatalytic oxidation of thiophene (*ca.* 40%), and the conversion was slightly improved by loading only 0.05 wt% Ni cocatalyst (*ca.* 43%) or 0.5 wt% CuO cocatalyst (*ca.* 42%). Most interestingly, when 0.05 wt% Ni and 0.5 wt% CuO were co-loaded on $BiVO_4$, the conversion was markedly enhanced to *ca.* 94.5%, much higher than those of Ni/$BiVO_4$ and CuO/$BiVO_4$. The conversion was also improved greatly when Ni and CoO_x were co-loaded onto $BiVO_4$, compared with Ni/$BiVO_4$ and CoO_x/$BiVO_4$ alone. A similar trend was observed for Ni–CoO_x/$BiVO_4$ catalyst but not for Co–NiO_x/$BiVO_4$ alone.

According to the abovementioned results, Ni–CuO/$BiVO_4$ turned out to be the most effective photocatalyst for the photocatalytic oxidation of thiophene. The synergistic effect of cocatalysts on $BiVO_4$ is very favorable for improving the photocatalytic activity of thiophene oxidation. It is also implied that the suitable energy level position of metals may be very important when choosing dual cocatalysts.

Fig. 7 shows the time course of photocatalytic oxidation of thiophene on $BiVO_4$, CuO/$BiVO_4$, Ni–CuO/$BiVO_4$ and Pt–RuO_2/$BiVO_4$. After 3 h of visible light irradiation, the residual thiophene concentration (C/C_0) was *ca.* 58% on $BiVO_4$, *ca.* 56% on

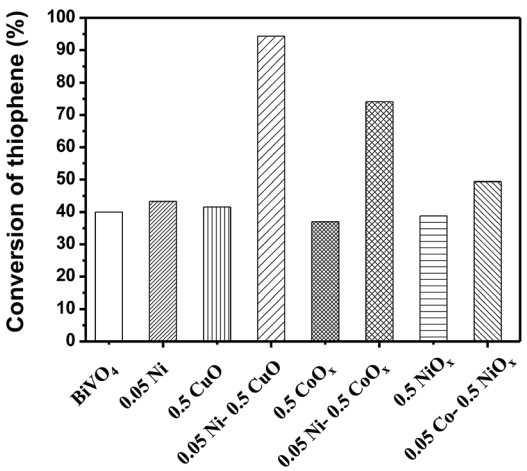

Fig. 6 Photocatalytic oxidation of thiophene on $BiVO_4$ and $BiVO_4$ loaded with various cocatalysts under visible light irradiation ($\lambda \geq 420$ nm). Herein 0.5 Cu represents 0.5 wt% CuO/$BiVO_4$, 0.05 Ni–0.5 Cu represents 0.05 wt% Ni–0.5 wt% CuO/$BiVO_4$, and so on… Reaction conditions: $[\text{sulfur content}]_{\text{initial}}$ = 600 ppm; the concentration of photocatalyst: 1 g L^{-1}; O_2 (bubbled into the system); temperature: 10 ± 2 °C; reaction time: 3 h.

$CuO/BiVO_4$, *ca.* 5% on Ni–$CuO/BiVO_4$, and *ca.* 1% on Pt–$RuO_2/BiVO_4$. The rate of degradation of thiophene with Ni–$CuO/BiVO_4$ catalyst was extremely fast compared with $BiVO_4$ and $CuO/BiVO_4$. In our previous study, thiophene (600 ppm) could be almost completely converted (*ca.* 99%) in 3 h for the optimized 0.03 wt% Pt–0.01 wt% $RuO_2/BiVO_4$ catalyst.[5] Under the same experimental conditions, the performance of the photocatalyst 0.05 wt% Ni–0.5 wt% $CuO/BiVO_4$ was very close to that of 0.03 wt% Pt–0.01 wt% $RuO_2/BiVO_4$. According to the above-mentioned results, we can conclude that the synergistic effect of cocatalysts Ni and CuO on $BiVO_4$ is very favorable for improving the photocatalytic activity of thiophene oxidation.

On the other hand, the noble-metal-free catalyst possess a high photocatalytic activity close to Pt–$RuO_2/BiVO_4$, which is very important for further application requirements for ultra-low sulfur-containing fuels.

3.3 The proposed reaction mechanism

To investigate the reaction process of photocatalytic oxidation of thiophene on Ni–$CuO/BiVO_4$, we used XPS to investigate the combined-state of the Cu element on photocatalyst after the reaction. Fig. 8 shows the asymmetrical X-ray photoelectron spectrum of Cu 2p levels of Ni–$CuO/BiVO_4$ catalyst after the photocatalytic oxidation reaction. Cu $2p_{3/2}$ and Cu $2p_{1/2}$ XPS of the used catalyst exhibited sharp peaks at 932.4 eV and 952.2 eV, respectively, without any shift in the binding energy (BE). A strong satellite peak was observed on the higher BE side above 940 eV indicating the existence of divalent Cu.[32] In addition, CuO $2p_{3/2}$ and CuO $2p_{1/2}$ XPS also exhibited small peaks at 933.6 eV and 953.6 eV respectively. The results indicate that a certain amount of CuO_x (mixture of CuO and metal Cu) remained on the surface of the used catalyst. Cu^{2+} is thus partially reduced to metallic copper (Cu^0) and/or Cu^{1+} in the photocatalytic oxidation reaction.

In order to convert the XPS intensity ratio into the surface atomic ratio, the following expression was applied:[33]

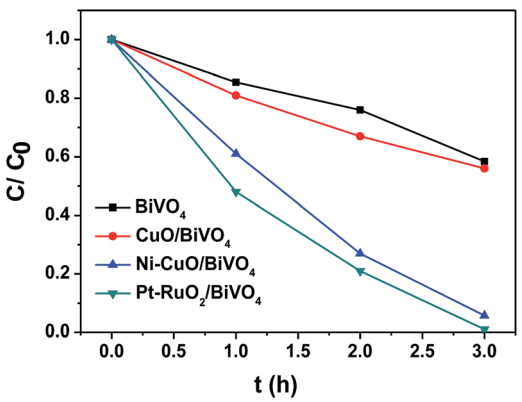

Fig. 7 Photocatalytic oxidation of thiophene on $BiVO_4$ and $BiVO_4$ loaded with various cocatalysts under visible light irradiation ($\lambda \geq 420$ nm). Reaction conditions: $[\text{sulfur content}]_{\text{initial}} = 600$ ppm; the concentration of photocatalyst: 1 g L^{-1}; O_2 (bubbled into the system); temperature: 10 ± 2 °C; reaction time: 3 h.

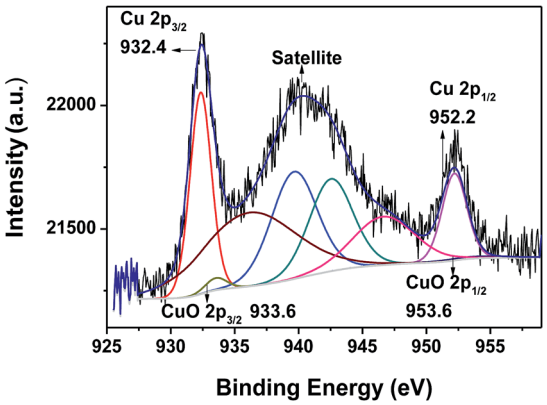

Fig. 8 Cu 2p XPS of Ni–$CuO/BiVO_4$ catalyst after the photocatalytic oxidation reaction.

$$(Cu/Cu^{2+})\ XPS = C(I_{Cu\ 2p_{3/2}}/I_{Cu2p_{3/2}{}^{2+}})$$

where I represents the peak area and C is the relative atomic sensitivity factor ($C = 1$ for the same element). The measured intensity for Cu/Cu^{2+} peaks is shown in Table 1. According to the above expression, the surface atomic ratio Cu/Cu^{2+} was 16.6. This means that most CuO of fresh photocatalyst is reduced to metallic copper (Cu^0) and/or Cu^{1+} after the photocatalytic oxidation reaction.

To clarify the reaction mechanism for the photocatalytic oxidation of thiophene on Ni–$CuO/BiVO_4$, the ESR spin-trap technique (with DMPO) was employed to probe the active oxygen species generated under the illumination. Fig. 9 shows the ESR signals obtained from the *in situ* photocatalytic reaction. The ESR signals that appeared in the presence of photocatalysts were centered at $g = 2.0065$, which can be assigned to oxygen species.[34] No ESR signals were observed either when the photocatalyst was absent or the reaction was performed with $BiVO_4$ in the dark. After light irradiation, a sextet ESR signal was observed that is assigned to DMPO–$O_2^{\bullet-}$. The hyperfine splittings were $a_N = 1.27$ mT, $a_H^{\beta} = 0.99$ mT and $a_H^{\gamma} = 0.14$ mT, where a_N, a_H^{β} and a_H^{γ} are hyperfine splitting constants of nitroxyl nitrogen, one β-hydrogen and one γ-hydrogen, respectively.[6,35,36] These results provide evidence of $O_2^{\bullet-}$ formed in the presence of photocatalysts $BiVO_4$ and Ni–$CuO/BiVO_4$. May be the $^{\bullet}OH$, which has strong oxidizing ability, was also generated with the illumination, but the characteristic quartet peaks of the DMPO–OH adduct were submerged in the sextet signal of DMPO–$O_2^{\bullet-}$ adduct. Moreover, the signals of $O_2^{\bullet-}$ generated after illumination on Ni–$CuO/BiVO_4$ for 8 min were more obvious than those for $BiVO_4$. This might be one reason for the higher photocatalytic activity of Ni–$CuO/BiVO_4$. During the photocatalytic oxidation reaction with Ni–$CuO/BiVO_4$ catalyst, more active oxygen species were generated under the illumination for the oxidation of pollutants. After 16 min of illumination, the signals intensity was decreased. This is due to the consumption of the dissolved O_2 and the oxidation of DMPO–$O_2^{\bullet-}$ adduct by h^+ generated during the illumination. In conclusion, for Ni–$CuO/BiVO_4$, the simultaneous existence of reduction cocatalyst and oxidation cocatalyst is beneficial for efficient separation and

Table 1 BE (eV) of Cu 2p levels and surface atomic ratio of Ni–CuO/$BiVO_4$ catalyst after the photocatalytic oxidation reaction

Item	Cu $2p_{3/2}$	Cu $2p_{1/2}$	CuO $2p_{3/2}$	CuO $2p_{1/2}$	Satellite	Cu/CuO (atomic ratio)
BE (eV)	932.4	952.2	933.6	953.6	941.0	
Peak area	1744.8	872.4	105.4	52.7	—	16.6

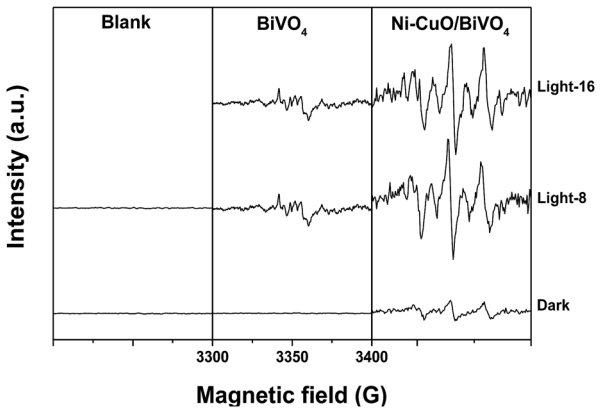

Fig. 9 *In situ* ESR spectra of DMPO–$O_2^{\bullet-}$ generated in the photocatalytic oxidation reaction of thiophene with different photocatalysts. The sample tested without photocatalyst is denoted as "Blank". The signals obtained without light irradiation are denoted as "Dark". The signals obtained after irradiating for 8 min are denoted as "Light-8", similarly, for 16 min named "Light-16".

transport of the photo-excited electrons and holes, respectively. The production of $O_2^{\bullet-}$ and photo-excited holes can be enhanced simultaneously, resulting in the high photocatalytic activity of thiophene oxidation.

According to the results of XPS and ESR, we propose a reaction mechanism for the photocatalytic oxidation of pollutants on Ni–CuO/$BiVO_4$ photocatalyst. The right part in Scheme 1 illustrates the charge transfer processes between the Ni, Cu based dual cocatalysts and semiconductor $BiVO_4$. First, under the visible light irradiation, electron–hole pairs are photo generated in $BiVO_4$. Due to the energy level matching of $BiVO_4$ and CuO, the photo-generated electron transfer from the conduction band of $BiVO_4$ to that of CuO, and photo-generated holes transfer from the valence band of $BiVO_4$ to that of CuO. In this electron transfer process, CuO can be partially reduced to Cu_2O. Second, because of the energy level matching of CuO and

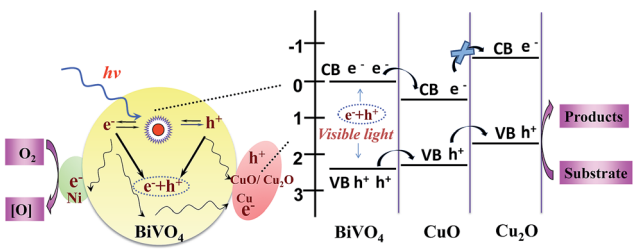

Scheme 1 Schematic of the mechanism for photocatalytic oxidation of pollutants on Ni–CuO/$BiVO_4$ photocatalyst.

Cu_2O, the photo-generated holes transfer from the valence band of CuO to that of Cu_2O, but the photo-generated electrons cannot transfer. Herein, Cu_2O/CuO acts as the oxidation cocatalyst for generated hole transfer. Third, the Cu_2O acts as a barrier for the electrons of $BiVO_4$/CuO to reach the Cu_2O surface and the electrons are trapped in CuO, which may be the reason for the valence of most Cu being Cu^0 for the used photocatalyst (XPS results). Consequently, most holes can reach the Cu_2O/CuO and substrate interface, and thus, the charge separation and transport in photocatalysts is greatly accelerated without recombination, leading to the oxidation of pollutants. On the other side (as shown in the left part in Scheme 1), Ni^0 and Cu^0 with low Fermi levels on the surface of $BiVO_4$ act as the reduction cocatalyst, and thus photo-generated electrons transfer to O_2 *via* Ni (0) and Cu (0) cocatalysts, where superoxide species $O_2^{\bullet-}$ is formed when O_2 reacts with the photo-generated electrons. Namely, the adsorbed oxygen acts as an electron trap that efficiently inhibits electron–hole recombination.[37] Then, $^{\bullet}OH$, which has a strong oxidation ability, might be generated *via* reaction of OH^- with holes in the reaction system under the illumination. The active oxygen species can react with pollutant molecules in the presence of Ni–CuO/$BiVO_4$ catalyst. Thus, the series of photocatalytic oxidation reactions are accelerated on Ni/Cu and CuO/Cu_2O co-loaded on $BiVO_4$ catalyst. The synergistic effect of CuO acting as an oxidation cocatalyst and Ni acting as a reduction cocatalyst is beneficial for the efficient separation and transfer of the photo-excited electrons and holes, being responsible for the high photocatalytic oxidation activity of pollutants.

4. Conclusions

The visible light responsive photocatalyst $BiVO_4$ co-loaded with noble-metal-free Ni and CuO can achieve over 94% conversion of thiophene oxidation under visible light irradiation using molecular oxygen as the oxidant. This high activity of Ni–CuO/$BiVO_4$ was also successfully presented in photocatalytic oxidation of organic dyes. Dual cocatalysts Ni and CuO showed a strong synergistic effect on the enhanced photocatalytic activity. The noble-metal-free catalyst possessed high photocatalytic activity close to Pt–RuO_2/$BiVO_4$ (in the same condition), which is very important for further application requirements in industry. XPS and ESR measurements showed that the activation of molecular oxygen and oxidation of pollutants molecule simultaneously take place on Ni/Cu and CuO/Cu_2O co-loaded on $BiVO_4$ catalyst. Herein, Ni/Cu acted as the reduction cocatalyst for photo-generated electron transfer, while CuO/Cu_2O acted as the oxidation cocatalyst for photo-generated hole transfer. The co-existing low-cost dual

cocatalysts thus play the significant role in greatly enhancing the photocatalytic oxidation activity. The visible light responsive semiconductor loaded with earth-abundant dual cocatalysts has great potential in both solar energy conversion and further industrial applications.

Acknowledgements

This study was financially supported by the National Natural Science Foundation of China (Grant No. 21603025, 11274057, 11474046, 21506203) and Open Project of State Key Laboratory of Catalysis, Dalian Institute of Chemical Physics, Chinese Academy of Sciences (Grant No. N-15-06). The authors thank Prof. Can Li of Dalian Institute of Chemical Physics (Chinese Academy of Sciences) very much for his advice in experiment and discussion.

Notes and references

1 S. J. A. Moniz, S. A. Shevlin, D. J. Martin, Z. X. Guo and J. W. Tang, *Energy Environ. Sci.*, 2015, **8**, 731.
2 Z. J. Sun, H. F. Zheng, J. S. Li and P. W. Du, *Energy Environ. Sci.*, 2015, **8**, 2668.
3 B. Y. Zhang, Z. X. Jiang, J. Li, Y. N. Zhang, F. Lin, Y. Liu and C. Li, *J. Catal.*, 2012, **287**, 5.
4 Y. Z. Zhen, J. Li, D. J. Wang, F. Fu and G. L. Xue, *J. Inorg. Mater.*, 2015, **30**, 408.
5 F. Lin, D. E. Wang, Z. X. Jiang, Y. Ma, J. Li, R. G. Li and C. Li, *Energy Environ. Sci.*, 2012, **5**, 6400.
6 F. Lin, Y. N. Zhang, L. Wang, Y. L. Zhang, D. E. Wang, M. Yang, J. H. Yang, B. Y. Zhang, Z. X. Jiang and C. Li, *Appl. Catal., B*, 2012, **127**, 363.
7 F. Lin, Z. X. Jiang, N. F. Tang, C. Zhang, Z. P. Chen, T. F. Liu and B. Dong, *Appl. Catal., B*, 2016, **188**, 253.
8 F. Chen, J. C. Zhao and H. Hidaka, *Res. Chem. Intermed.*, 2003, **29**, 733.
9 X. Lin, X. Y. Guo, W. L. Shi, F. Guo, G. B. Che, H. J. Zhai, Y. S. Yan and Q. W. Wang, *Catal. Commun.*, 2015, **71**, 21.
10 X. Lin, Y. S. Wang, J. Zheng, C. Liu, Y. Yang and G. B. Che, *Dalton Trans.*, 2015, **44**, 19185.
11 J. W. Tang, Z. G. Zou and J. H. Ye, *Angew. Chem., Int. Ed.*, 2004, **43**, 4463.
12 J. F. Ma, J. Zou and L. Y. Li, *Appl. Catal., B*, 2014, **144**, 36.
13 F. Guo, W. L. Shi, X. Lin, X. Yan, Y. Guo and G. B. Che, *Sep. Purif. Technol.*, 2015, **141**, 246.
14 X. Lin, X. Y. Guo, W. L. Shi, L. N. Zhao, Y. S. Yan and Q. W. Wang, *J. Alloys Compd.*, 2015, **635**, 256.
15 X. Lin, D. Xu, J. Zheng, M. S. Song, G. B. Che, Y. S. Wang, Y. Yang, C. Liu, L. N. Zhao and L. M. Chang, *J. Alloys Compd.*, 2016, **688**, 891.
16 M. M. Liu, F. Y. Li, Z. X. Sun, L. Xu, Y. F. Song and A. Munventwali, *RSC Adv.*, 2015, **5**, 47314.
17 A. Y. Meng, J. Zhang, D. F. Xu, B. Cheng and J. G. Yu, *Appl. Catal., B*, 2016, **198**, 286.
18 H. J. Yan, J. H. Yang, G. J. Ma, G. P. Wu, X. Zong, Z. B. Lei, J. Y. Shi and C. Li, *J. Catal.*, 2009, **266**, 165.
19 S. S. K. Ma, K. Maeda, R. Abe and K. Domen, *Energy Environ. Sci.*, 2012, **5**, 8390.
20 K. Maeda, T. Ohnoa and K. Domen, *Chem. Sci.*, 2011, **2**, 1362.
21 W. J. Foo, C. Zhang and G. W. Ho, *Nanoscale*, 2013, **5**, 759.
22 B. Zhou and J. H. Qu, *Appl. Catal., B*, 2010, **99**, 214.
23 F. X. Zhang, A. Yamakata, K. Maeda, Y. Moriya, T. Takata, J. Kubota, K. Teshima, S. Oishi and K. Domen, *J. Am. Chem. Soc.*, 2012, **134**, 8348.
24 G. C. Bi, J. Q. Wen, X. Li, W. Liu, J. Xie, Y. P. Fang and W. W. Zhang, *RSC Adv.*, 2016, **6**, 31497.
25 Y. Xu and R. Xu, *Appl. Surf. Sci.*, 2015, **351**, 779.
26 T. Pham, C. Nguyen-Huy and E. W. Shin, *Appl. Surf. Sci.*, 2016, **377**, 301; J. Q. Wen, X. Li, H. Q. Li, S. Ma, K. L. He, Y. H. Xu, Y. P. Fang, W. Liu and Q. Z. Gao, *Appl. Surf. Sci.*, 2015, **358**, 204.
27 L. L. Li, B. Cheng, Y. X. Wang and J. G. Yu, *J. Colloid Interface Sci.*, 2015, **449**, 115.
28 Q. Z. Wang, G. X. Yun, Y. Bai, N. An, Y. T. Chen, R. F. Wang, Z. Q. Lei and W. F. Shangguan, *Int. J. Hydrogen Energy*, 2014, **39**, 13421.
29 Q. Q. Hu, J. Q. Huang, G. J. Li, J. Chen, Z. J. Zhang, Z. H. Deng, Y. B. Jiang, W. Guo and Y. G. Cao, *Appl. Surf. Sci.*, 2016, **369**, 201.
30 J. Q. Yu and A. Kudo, *Adv. Funct. Mater.*, 2006, **16**, 2163.
31 W. Z. Yin, W. Z. Wang, L. Zhou, S. M. Sun and L. Zhang, *J. Hazard. Mater.*, 2010, **173**, 194.
32 S. Velu, K. Suzuki, M. Vijayaraj, S. Barman and C. S. Gopinath, *Appl. Catal., B*, 2005, **55**, 287.
33 G. Fierro, M. L. Jacono, M. Inversi, R. Dragone and P. Porta, *Top. Catal.*, 2000, **10**, 39.
34 S. Leonard, P. M. Gannett, Y. Rojanasakul, D. Schwegler-Berry, V. Castranova, V. Vallyathan and X. L. Shi, *J. Inorg. Biochem.*, 1998, **70**, 239.
35 J. R. Harbour and M. L. Hair, *J. Phys. Chem.*, 1978, **82**, 1397.
36 Y. Huang, J. Li, W. Ma, M. Cheng, J. Zhao and J. C. Yu, *J. Phys. Chem. B*, 2004, **108**, 7263.
37 J. Robertson and T. J. Bandosz, *J. Colloid Interface Sci.*, 2006, **299**, 125.